5th International Conference on Experimental Fluid Mechanics ICEFM 2018 Munich
Munich, Germany, July 2-4, 2018

Flow reversal in turbulent boundary layers with varying pressure gradients

Christian E. Willert[1*], Christophe Cuvier[2], Julio Soria[3], Jean Marc Foucaut [2], Jean Philippe Laval

[1] DLR Institute of Propulsion Technology, German Aerospace Center, Köln, Germany

[2] Université Lille Nord de France, LMFL - Laboratoire de Mécanique des Fluides de Lille, FRE CNRS 2017, Centrale Lille, ENSAM, ONERA, Villeneuve d'Ascq, France

[2] Monash University, LTRAC, Department of Mechanical and Aerospace Engineering, Clayton Campus, Melbourne, Australia

[*] chris.willert@dlr.de

Abstract

This contribution describes detailed PIV measurements obtained in turbulent boundary layers in order to capture rarely occurring flow reversals within the viscous sublayer, which previously have been observed in both experiments and direct numerical simulations. Due to their confinement to the viscous sublayer along with their rare occurrence on the order of 10^{-4}, any statistical investigation requires very large data sets exceeding 10^5 samples. In the present investigation, this was achieved by capturing long PIV records using image high magnification near unity. To investigate the influence of Reynolds number and pressure gradient, the measurements were performed in turbulent boundary layers in both zero pressure gradient (ZPG) and adverse pressure gradient (APG) conditions. The measurements were conducted in the TBL wind tunnel of Lille which features a test section length of 20 m and cross-section of 2×1 m^2. A ramp model placed inside the tunnel introduced APG conditions. Both visual inspection of the raw data and a dedicated processing scheme to retrieve the unsteady wall shear stress were used to quantify the flow reversal events. The occurrence of the self-similar flow reversals was found to weakly depend on the Reynolds numbers in ZPG and roughly doubled in frequency in the APG condition.

1 Introduction

Wall bounded flows submitted to an adverse pressure gradient (APG) are common in many engineering applications, especially in transportation vehicles, such as on the suction side of airfoils. When the strength of the APG is high enough, it can lead to a flow separation, which decreases the performance (increased drag, decreased lift). In the frame of improving the performance of vehicle/aircraft, flow control strategies are tested but most of them try to completely reorganize the flow. At this time, this requires a significant amount of energy which often is not optimal or sometimes even unrealistic. It is therefore important to improve the understanding of the organization of APG flows and to understand the physics of the flow separation which is the basis for new concepts of flow control. The objective of the present investigation is to bring further insights about APG flow organization. In this context, the rare reverse flow events which appear very close to the wall of turbulent boundary layers (TBL) are investigated in detail in order to understand their possible connection with large scale structures which develop in the external region. These events were firstly evidenced by direct numerical simulations (DNS) of channel flow and zero pressure gradient (ZPG) TBL and was characterized in detail by Lenaers et al. (2012), through a channel flow simulation at low Reynolds numbers and more recently by Jalalabadi and Sung (2018) for DNS of a pipe flow.

Experimentally, reverse flow events are very difficult to measure as requires high spatial resolution measurements in close proximity to the wall. These structures are 20-40 viscous units in length and remain within the viscous sublayer Lenaers et al. (2012); Vinuesa et al. (2017). At the same time, very large sample counts are required as their probability is small, typically of the order of 0.1% or less. The existence

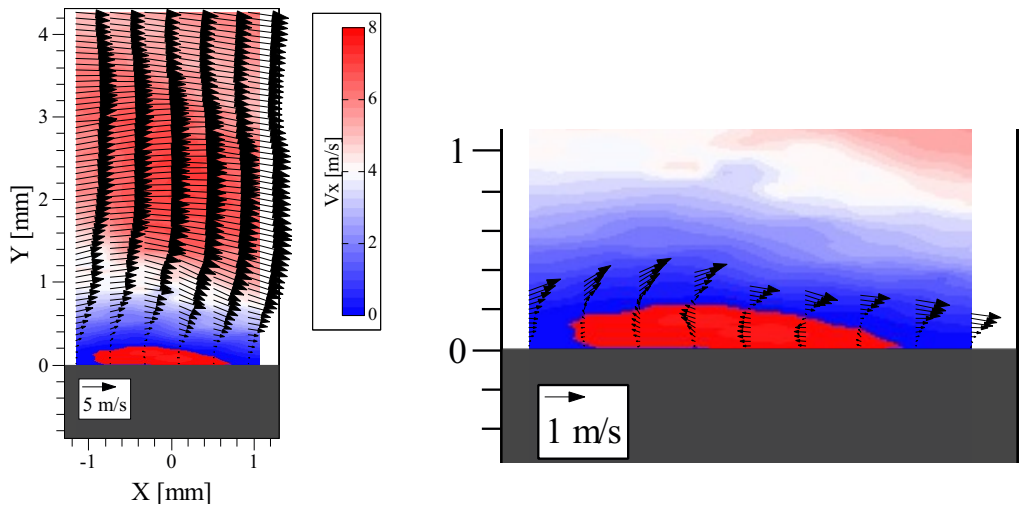

Figure 1: Single reverse flow event, indicated by the red patch above the wall at y=0 captured in the APGTBL at $U_\infty = 9$ m/s. PIV processing with sampling windows of 24×8 pixel ($6.1^+ \times 2.0^+$) with vertical vector spacing of $\delta x = 0.5^+$. The length of the structure is $x = 35^+$, its height $y = 4.5^+$.

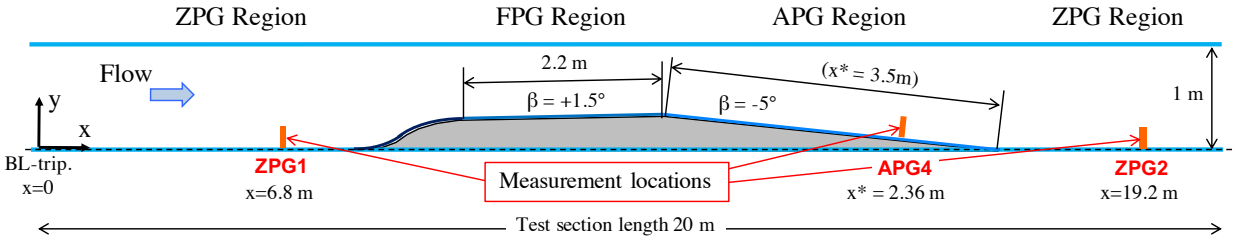

Figure 2: Wind tunnel test section and measurement locations. Measurements at ZPG2 were performed without the presence of the ramp model

and topology of reverse flow events and their connection with surrounding flow can nowadays be obtained through particle image velocimetry (PIV) and is chosen for the present investigation.

In the frame of the recent EuHIT project Large Scale Structures under Adverse Pressure Gradient (Cuvier et al. (2017)) high magnification PIV already provided some experimental evidence of these reverse flow events, however with limited spatial resolution and with small sample counts (Willert et al. (2018). The aim of the present study was to specifically capture the reverse flow events using several different PIV implementations to further understand the underlying mechanisms of their appearance, in particular, under in the influence of different pressure gradients.

A typical example of this flow feature is provided in Fig. 1. In agreement with previous literature on the subject, in particular DNS data, the size of the enclosing zero-velocity streamline of the flow structures is roughly 20-40 wall units in streamwise direction and limited to the viscous sublayer ($y < 5^+$). While difficult to measure, DNS data suggests a spanwise dimension similar to the streamwise extent.

In Fig. 1 and in the remainder of the text, the streamwise direction is denoted with X, the wall-normal by Y and the spanwise direction by Z. Finally, a superscript + denotes scaling in viscous units $l^* = \nu/u_\tau au$ where ν is the kinematic viscosity of air and u_τ is the friction velocity defined as $u_\tau = (\nu \partial u/\partial y)^{0.5}$. Here the velocity gradient $\partial u/\partial y$ is the wall shear rate at the wall at $y = 0$ estimated through a specific particle image analysis described within this contribution.

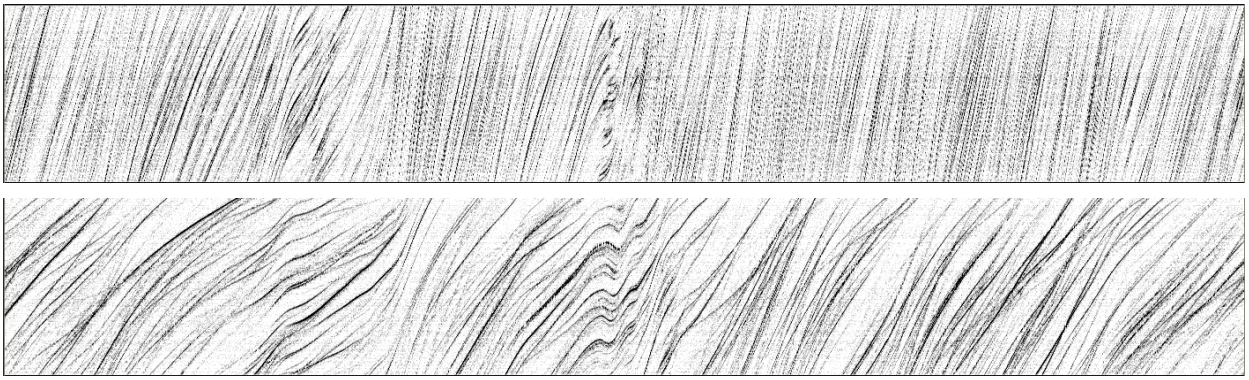

Figure 3: Particle streak images compiled from high-speed particle image recordings by extracting a fixed row of pixels from each image. The top image is at a wall distance of 180 μm ($4.6\,y^+$), the lower image at 55 μm ($1.3\,y^+$). The vertical axis coincides with the streamwise axis X whereas the horizontal axis corresponds to time - here 0.056 s (1400 samples). The signature of a single reverse flow event can be seen near the middle of the images.

2 Experimental facility and methods

The measurements are performed in a closed-loop wind tunnel of the LMLF at Centrale de Lille. The testsection has total length of $x = 20$ m with a spanwise width of $z = 2$ m and height $y = 1$ m. Designed for long-duration hotwire measurements, the temperature of the flow is maintained to within $\pm 0.1\circ$C using a heater/chiller system. Measurements are first performed at two streamwise positions ($x = 6.8$ m and $x = 19.2$ m) to study the reverse flow with minimal pressure gradient ($\partial p/\partial x^+ \approx -1.4\times10^{-4}\ldots-2.0\times10^{-4}$) at two different free stream velocities. For measurements under the influence of the adverse pressure gradient a ramp is installed in the test section as outlined in Fig. 2. Further details on the facility and the ramp can be found in Cuvier et al. (2017).

The current investigation relies on data acquired in a streamwise wall normal plane (XY) using two-component, two-dimensional (2C-2D) particle image velocimetry (PIV). For image recording, a high- speed camera (Miro310, Vision Research) and a sCMOS double-frame PIV camera (Edge5.5, PCO AG) was used.

In spite of the large working distance of more than 1 m, an image magnification $m > 1.0$ was achieved using f=300 mm telephoto lenses (Nikon Nikkor 300/4.0) together with tele-converters (Nikon TC2.1) that double the effective focal lengths to 600 mm with the caveat of proportionlly reducing the numerical aperture. In addition, the aperture of the lenses had to be stepped down by at least one more f-stop to $f_{\#,\mathrm{eff}}11$ to reduce the diffraction size of the imaged particle (smaller particle images). In order to prevent image diffraction near the glass wall due to a partially occluded lens aperture, the optical axis was inclined by about 1° with respect to the wall.

Using a high-speed laser (NanioAir, Innolas Photonics) the particles were illuminated with a light sheet of about $\delta x = 2$ mm width and thickness of about $\delta z = 0.2$ mm (as measured with burn paper). The pulse energy at 20 kHz is 0.5 μJ/pulse with a corresponding fluence of about 1.25 J/mm^2 and a pulse width on the order of 20 ns.

The windtunnel was continuously seeded with a water glycol mixture using an evaporation-condensation fogger producing droplets in the range $1-2\,\mu$m. The seeding density was estimated at 3000 particles/mm^3.

2.1 Estimation of the mean and unsteady wall shear stress

The wall shear rate $S = \partial u/\partial y$ and with it the wall shear stress $\tau_w = \rho\nu\partial u/\partial y$ is determined from the near-wall, streamwise velocity u obtained through the measurement of particle motion in the image data. The particles are typically in the 12 μm range which is more than one order of magnitude smaller than the viscous scales in the flow ($l = \nu/u_\tau = 40120\,mu$m). Given a particle response time of $t_p \approx 10\mu$s or $t_p \approx 0.03t^+$ the Stokes number $\mathrm{St} = t_p U d^1$ based on friction velocity $u_t au$ and viscous sublayer thickness $d = 5\,y^+$ reduces to 0.005, which indicates that the particles follow the flow faithfully.

If sufficient velocity estimates are available from within the viscous sublayer, preferably in the range $0 < y < 3^+$, the velocity gradient can be estimated through finite differences (Willert (2015)). Here it is

worth noting that the magnification factor relating physical space to image space is not required since it cancels out in the estimation of the gradient. This makes the measurement approach particularly attractive as it only requires the knowledge of the time separation between the image recordings, Δt.

The near wall velocity can be determined from single lines of wall-parallel pixel rows using one- dimensional cross-correlation. This can be achieved very efficiently by compiling all pixel rows in a common image such as presented in Fig. 3. If the sequence is temporally well resolved, the movement of particles shows up as streaks. The slope of these streaks is a direct indication of their actual velocity as projected onto the pixel row. Movement normal to the pixel row or outside of the light sheet plane results fading or appearing of streaks. Changes in slope indicate acceleration or deceleration.

For the correlation analysis adjacent rows (or separated by 1 or more) are cross-correlated uses 1-D FFTs performed in parallel. A three-point Gaussian peak fit locates the maximum correlation with sub-pixel accuracy in analogy to conventional 2-C PIV processing. For a continuous image sequence of N images this results in (N-1) velocity estimates for each pixel row above the wall. Along with the data from the other rows the mean velocity profile can be determined and is used to estimate the mean velocity gradient for the image sequence using a linear least squares fit (see e.g. Figure 4, left). It should be noted that the length of the correlation samples, typically the image width, defines the domain over which the velocity is averaged, so there will be a smoothing influence on the recovered data.

In a second step the unsteady wall shear rate is determined by performing a linear least squares fit using the group of velocity estimates for each time instant. This data can then be used to provide statistical estimates of the wall shear stress, such as its RMS, skew and flatness (kurtosis). Normalized probability density functions (PDFs) of the unsteady wall shear stress, such as shown in Fig. 4, allow for a visual comparison of the retrieved data for the various flow conditions. Here the logarithmic scaling of the probability axis reveals features such as rarely occurring reverse flow events ($\tau_w < 0$) or very fast streaking events at the upper end of the PDF.

3 Results and discussion

The statistics of the near-wall velocity and related quantities are summarized in Table 1. For the ZPG the higher moments (skew and flatness) and the ratio of the RMS and mean shear rate show no noticeable dependence on Reynolds number. Under the influence of the APG these quantities show a slight increase. The probability density distributions for three relevant flow conditions are shown in Fig. 5 and indicate two aspects: (1) with increasing the Reynolds number influence the PDF broadens (red vs. blue line), and (2) the adverse pressure gradient broadens the PDF even further. Here the probability of zero and negative wall shear stress increases significantly from about 1×10^{-4} in ZPG to about 1×10^{-3} in the APG. An influence of Reynolds number for ZPG conditions cannot be observed as clearly as for the lower Reynolds numbers of the DNS results provided in the literature (e.g. Diaz-Daniel et al. (2017) and Örlü and Schlatter (2011)).

For the estimation of the actual number of reverse flow events, manual scanning of the streak images of the type shown in Fig. 3 was performed. The recovered reverse flow data is summarized in Table 2. The frequency of event occurrence increases both with Reynolds number and under the influence of the adverse pressure gradient. Determining the probability of the reverse flow events from the event counts is must take into account the fact that the data is temporally correlated and requires an estimate of the actual number of independent samples. For the present analysis, the mean temporal spacing t rev of the reverse flow events is normalized with the width of the field of view ($\Delta x \approx 2\,\mathrm{mm}$) and the edge velocity U_∞. Based on this estimate the reverse flow probability approximately doubles under the influence of the APG. An influence of the outer flow velocity on this probability presently cannot be conclusively determined.

4 Conclusion

Over the course of one month a PIV measurement campaign acquired an extensive data base of the near-wall flow of a turbulent boundary layer at both near-zero pressure gradient and adverse (positive) pressure gradient. The number of samples in excess of 10^5 for all conditions studied is believed to be sufficient to allow a more quantitative assessment regarding the statistics of rarely occurring phenomena such as flow reversal. Beyond the high-magnification data presented here, the data base includes measurements at similar magnifications using large format sensors (5.5 MPixel and 29 MPixel) to assess the interaction of reverse flow events in larger areas of interest. Stereoscopic PIV measurements of the spanwise, wall-normal plane

Table 1: Near-wall velocity statistics

	ZPG, $x = 6.8$ m		ZPG, $x = 19.2$ m		APG4, $x^* = 2.36$ m	
free stream velocity, U_∞	5 m/s	9 m/s	6 m/s	9 m/s	5 m/s	9 m/s
shear velocity, u_τ	0.204 m/s	0.343 m/s	0.232 m/s	0.340 m/s	0.181 m/s	0.322 m/s
viscous length, $l^* = \nu/u_\tau$	74 μm	44 μm	65 μm	44 μm	82 μm	46 μm
Re_τ	1 840	2 360	3 840	5 590	(n.a.)	(n.a.)
Re_θ	5 620	8 120	12 720	18 360	(n.a.)	(n.a.)
shear rate, $S = du/dy\|_0$	2 770 s^{-1}	7 860 s^{-1}	3 580 s^{-1}	7 690 s^{-1}	2 220 s^{-1}	6 960 s^{-1}
ratio, σ_s/S	0.43	0.42	0.42	0.43	0.46	0.47
skew(S)	1.09	1.05	1.04	1.13	1.24	1.20
flatness(S)	5.15	4.66	4.59	4.99	5.52	5.00
samples, N	220 000	400 000	950 000	3 920 000	2 410 000	3 000 000
width of sample domain, Δx	44^+	75^+	41^+	53^+	32^+	57^+

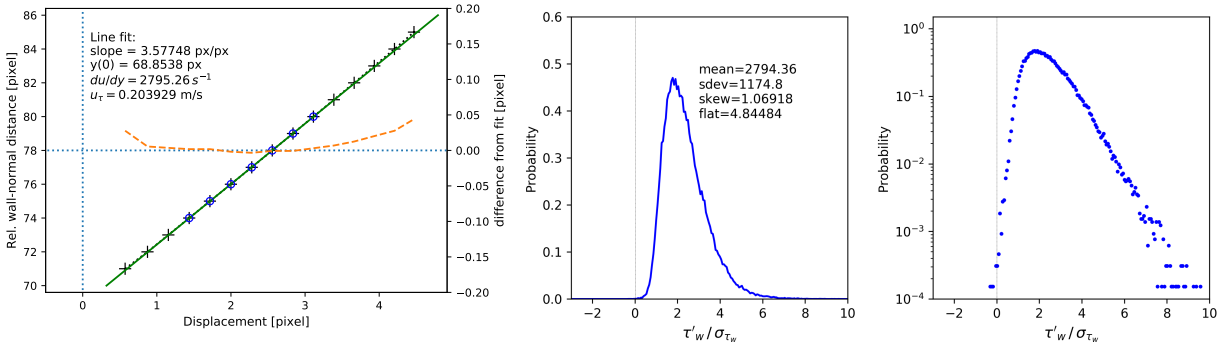

Figure 4: Left: estimation of the mean velocity gradient from the velocity profile using linear least squares fit. The (blue) circled symbols are used for the fit; the orange dashed line shows the deviation to the linear fit. Right: PDFs of the wall shear rate for a single image sequence in linear and linear-logarithmic representation. Values to the left of the vertical line at zero indicate negative shear stress events.

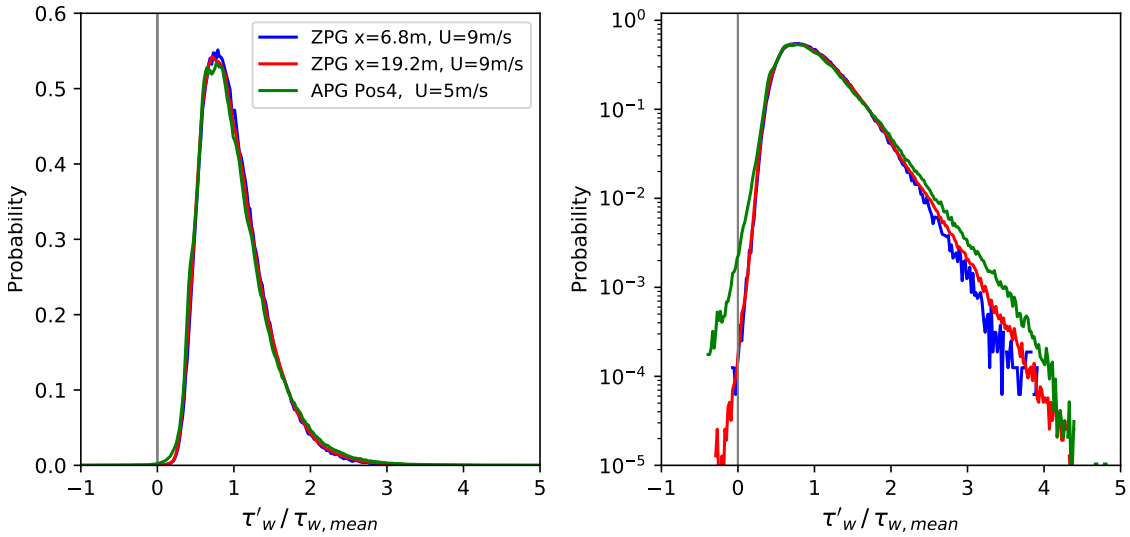

Figure 5: PDFs of the wall shear stress at streamwise positions $x = 6.8$ m ($Re_\tau = 2360$, blue), at x = 19.2 m ($Re_\tau = 5590$, red) and in the APG region (green)

Table 2: Statistics of reverse flow events

	ZPG, $x = 19.2$ m		APG4, $x^* = 2.36$ m	
free stream velocity, U_∞	6 m/s	9 m/s	5 m/s	9 m/s
reverse flow events	41	197	175	(380)[1]
number of images, N	952 000	3 920 000	2 410 000	3 000 000
number of sequences	13	42	33	36
total sequence duration	47.6 s	157 s	121 s	150 s
temporal event spacing	1.16 s	0.80 s	0.70 s	0.39 s
- - -, in viscous units	$4\,160t^+$	$6\,130t^+$	$1\,510t^+$	$2\,730t^+$
estimated probability	2.8×10^{-4}	2.7×10^{-4}	5.7×10^{-4}	5.5×10^{-4}

[1]) Estimated from analysis of 5 sequences

at high-magnification and high frame rates obtained in the APG region will allow the investigation of the spanwise flow field surrounding the reverse flow events.

The material presented herein is still subject to ongoing investigation as much of the data has yet to be processed in detail. This will include an assessment of the effects of spatial filtering on the estimation of the unsteady wall shear rate. For instance, the present PDFs given in Fig. 5 do not show APG data at $U_\infty = 9$ m/s due to the presence of spatial filtering artifacts and loss of signal at higher velocities. Also wall vibrations present on the APG ramp amounting to 1-2 wall units so far have not been accounted for and may also contaminate estimates of the wall shear rate. Further topics to be addressed in the future is the comparison of wall shear stress statistics and related power spectra with recently published DNS data, such as by Diaz-Daniel et al. (2017). Finally, the self-similar shape and surrounding flow topology of the reverse flow events will be assessed based on conditionally averaged flow fields such as performed by Jalalabadi and Sung (2018) on DNS data of a pipe flow.

References

Cuvier C, Srinath S, Stanislas M, Foucaut JM, Laval JP, Kähler CJ, Hain R, Scharnowski S, Schrder A, Geisler R, Agocs J, Röse A, Willert C, Klinner J, Amili O, Atkinson C, and Soria J (2017) Extensive characterisation of a high reynolds number decelerating boundary layer using advanced optical metrology. *Journal of Turbulence* 18:929–972

Diaz-Daniel C, Laizet S, and Vassilicos JC (2017) Wall shear stress fluctuations: Mixed scaling and their effects on velocity fluctuations in a turbulent boundary layer. *Physics of Fluids* 29:055102

Jalalabadi R and Sung HJ (2018) Influence of backflow on skin friction in turbulent pipe flow. *Physics of Fluids* 30:065104

Lenaers P, Li Q, Brethouwer G, Schlatter P, and Örlü R (2012) Rare backflow and extreme wall-normal velocity fluctuations in near-wall turbulence. *Physics of Fluids* 24:035110

Örlü R and Schlatter P (2011) On the fluctuating wall-shear stress in zero pressure-gradient turbulent boundary layer flows. *Physics of Fluids (1994-present)* 23:021704

Vinuesa R, Örlü R, and Schlatter P (2017) Characterisation of backflow events over a wing section. *Journal of Turbulence* 18:170–185

Willert C, Cuvier C, Foucaut J, Klinner J, Stanislas M, Laval J, Srinath S, Soria J, Amili O, Atkinson C, Kähler C, Scharnowski S, Hain R, Schröder A, Geisler R, Agocs J, and Röse A (2018) Experimental evidence of near-wall reverse flow events in a zero pressure gradient turbulent boundary layer. *Experimental Thermal and Fluid Science* 91:320 – 328

Willert CE (2015) High-speed particle image velocimetry for the efficient measurement of turbulence statistics. *Experiments in Fluids* 56:17